HHS Public Access

Author manuscript

Neurotoxicology. Author manuscript; available in PMC 2019 January 01.

Published in final edited form as:

Neurotoxicology. 2018 January ; 64: 185–194. doi:10.1016/j.neuro.2017.07.026.

Phosphatidylinositol 3 kinase (PI3K) modulates manganese homeostasis and manganese-induced cell signaling in a murine striatal cell line

Miles R. Bryan[1,2,3], **Michael A. Uhouse**[1,2,3], **Kristen D. Nordham**[1,2,3], **Piyush Joshi**[1,2,3], **Daniel I.R. Rose**[1,2,3], **Michael T. O'Brien**[1,2,3], **Michael Aschner**[6], and **Aaron B. Bowman**[1,2,3,4,5]

[1]Vanderbilt University Medical Center: Dept. of Pediatrics, Nashville, TN

[2]Vanderbilt University Medical Center: Vanderbilt Brain Institute, Nashville, TN

[3]Vanderbilt University Medical Center: Dept. of Neurology and Biochemistry, Nashville, TN

[4]Vanderbilt University Medical Center: Vanderbilt Kennedy Center, Nashville, TN

[5]Vanderbilt University Medical Center: Vanderbilt Center for Stem Cell Biology, Nashville, TN

[6]Albert Einstein College of Medicine, Bronx, NY

Abstract

In a recent study, we found that blocking the protein kinase ataxia telangiectasia mutated (ATM) with the small molecule inhibitor (SMI) KU-55933 can completely abrogate Mn-induced phosphorylation of p53 at serine 15 (p-p53) in human induced pluripotent stem cell (hiPSC)-differentiated striatal neuroprogenitors. However, in the immortalized mouse striatal progenitor cell line STHdh$^{Q7/Q7}$, a concentration of KU55933 far exceeding its IC_{50} for ATM was required to inhibit Mn-induced p-p53. This suggested an alternative signaling system redundant with ATM kinase for activating p53 in this cell line- one that was altered by KU55933 at these higher concentrations (i.e. mTORC1, DNApk, PI3K). To test the hypothesis that one or more of these signaling pathways contributed to Mn-induced p-p53 we utilized a set of SMIs (e.g. NU7441 and LY294002) known to block DNApk, PI3K, and mTORC1 at distinct concentrations. We found that the SMIs inhibit Mn-induced p-p53 expression near the expected IC_{50s} for PI3K, versus other known targets. We hypothesized that inhibiting PI3K to reduce intracellular Mn and thereby decrease activation of p53 by Mn. Using the cellular fura-2 manganese extraction assay (CFMEA), we determined that KU55933/60019, NU7441, and LY294002 (at concentrations near their IC_{50s} for PI3K) all decrease intracellular Mn (~50%) after a dual, 24-hour Mn and SMI exposure. Many pathways are activated by Mn aside from p-p53, including AKT and mTOR pathways. Thus, we explored the activation of these pathways by Mn in STHdh cells as well as the effects of other

Correspondence to: Dr. Aaron Bowman, Department of Pediatric Neurology, Vanderbilt University, Nashville TN, 37221, aaron.bowman@vanderbilt.edu.

pathway inhibitors. p-AKT and p-S6 activation by Mn is almost completely blocked upon addition of NU7441(5μM) or LY294002(7μM), supporting PI3K's upstream role in the AKT/mTOR pathway. We also investigated whether PI3K inhibition blocks Mn uptake in other cell lines. LY294002 exposure did not reduce Mn uptake in ST14A, Neuro2A, HEK293, MEF, or hiPSC-derived neuroprogenitors. Next, we sought to determine whether inhibition of PI3K blocked p53 phosphorylation by directly blocking an unknown PI3K/p53 interaction or indirectly reducing intracellular Mn, decreasing p-p53 expression. In-Cell Western and CFMEA experiments using multiple concentrations of Mn exposures demonstrated that intracellular Mn levels directly correlated with p-p53 expression with or without addition of LY294002. Finally, we examined whether PI3K inhibition was able to block Mn-induced p-p53 activity in hiPSC-derived striatal neuroprogenitors. As expected, LY294002 does not block Mn-induced p-p53 as PI3K inhibition is unable to reduce Mn net uptake in this cell line, suggesting the effect of LY294002 on Mn uptake is relatively specific to the STHdh mouse striatal cell line.

Keywords

Manganese; STHdh; neurotoxicity; manganese transport; PI3K; p53; LY294002; NU7441; KU55933; KU60019

1 Introduction

The element manganese (Mn) is critical for almost all forms of life, yet in excess can be extremely toxic. In humans and mouse models, Mn toxicity has been linked to Parkinsonian-like neurodegeneration including a condition known as manganism [1–3]. This critical axis of essentiality toxicity demands strict regulation of Mn in almost all biological systems. Although some is known about Mn regulation at in the gut, very little is known about its regulation at the neuronal level. Understanding the complexity of this system is caused, in part, by the fact that most metal transporters are highly promiscuous, capable of transporting many different ions. Some of these include transporters divalent metal transporter-1 (DMT-1), transferrin, Ferroportin, Huntingtin interacting protein (HIP)14, PARK9 and calcium channels. In addition, few of these exclusively transport Mn at relevant concentrations aside from some possible exceptions such as SLC30A10 [4].

The STHdh immortalized murine neuroprogenitor cell model is an ideal system to study neuronal Mn biology as the cellular fura 2 manganese extraction assay (CFMEA) was developed and rigorously tested in this system[5]. Cellular Mn uptake in the STHdh cells is robust and can occur at levels which are sub-toxic, yet exhibit sensitive activation of cell signaling pathways which are much less responsive in other neuronal systems. In addition, our previous findings on Mn-induced activation of AKT and ATM/p53 were conducted primarily using in this model system[6, 7].

Mn is necessary for the activity of many biologically indispensable enzymes including manganese superoxide disumutase (MnSOD), arginase, and glutamine synthetase and sufficient for the activation of many more including ataxia telangiectasia mutated (ATM) kinase. Both toxic and sub-toxic levels of Mn are known to stimulate several critical cell signaling pathways implicated across a broad variety of biological processes and disease

states [8–20]. In this study, we focus particularly on p53 and AKT/mTOR pathways that have not only been studied in the context of Mn toxicity but also extensively implicated in several neurodegenerative diseases including Parksinson's and Huntington's disease [21–29]. Activation by Mn allows ATM to phosphorylate P53, a tumor suppressor gene [30]. P53 functions most commonly to direct DNA repair, cell cycle arrest, and apoptosis—processes highly implicated in both cancer and neurodegeneration. AKT/mTOR pathways—canonically activated by upstream growth factors—are implicated across a wide variety of processes spanning glucose metabolism, cell proliferation, autophagy and apoptosis. Presently, the regulation of Mn within neurons is a "black box" with little known about how Mn is transported or sequestered within the brain. Thus, understanding the complete implications of Mn homeostasis on Mn-responsive proteins and processes or even how Mn activates specific proteins has been difficult to study. We sought to study how Mn acts to stimulate the aforementioned cell signaling pathways in a murine striatal neuroprogenitor model and whether these Mn-responsive cell signaling pathways could also modulate Mn levels within these cells.

2 Methods and Materials

2.1 Inhibitors and antibodies

The small molecule inhibitors (KU55933, KU60019, NU7441, and LY294002) were purchased from Tocris, reconstituted in DMSO, and stored at −80 degrees prior to experiments. The rapamycin and Torin 2 were generous gifts from Dr. Kevin Ess. Antibodies were purchased from Cell Signaling Technologies (p-AKT (Ser473) #4060, p-p53 (Ser15) #9286, p-S6 (Ser235/236) #2211, actin #4968S).

2.2 Cell culture

The immortalized, wild-type, murine striatal cell line ($STHdh^{Q7/Q7}$) were obtained from Coriell Cell Repository (Cambden, NJ). $STHdh^{Q7/Q7}$ immortalized murine striatal cells were cultured in Dulbecco's Modified Eagle Medium [D6546, Sigma-Aldrich, St. Louis MO] supplemented with 10% FBS [Atlanta Biologicals, Flowery Branch, GA], 2 mM GlutaMAX (Life Technologies, Carlsbad, CA), Penicillin-Streptomycin, 0.5 mg/mL G418 Sulfate (Life Technologies, Carlsbad, CA), MEM non-essential amino acids solution (Life Technologies, Carlsbad, CA), and 14mM HEPES (Life Technologies, Carlsbad, CA). They were incubated at 33°C and 5% CO_2. Cells were passaged before reaching greater than 90% confluency. The cells were split by trypsinization using 0.05% Trypsin-EDTA solution (Life Technologies, Carlsbad, CA) incubated for five minutes. One day prior to exposure, cells were plated in the appropriate cell culture plate type at 8×10^5 cells/mL for STHdh.

Neuro2A, HEK293, ST14A, and mouse embryonic fibroblasts (MEF) were cultured in DMEM with 4.5g/L glucose, L-glutamine, and sodium pyruvate with 10% FBS and penicillin/streptomycin. All cells were grown at 37°C and 5% CO_2. MEF cells were harvested from WT BL6-c57 mice between E12.5–E13.5. For CFMEA experiments, 3 separate MEF lines were used.

2.3 Islet-1 striatal neuroprogenitors derived from hiPSCs

Islet-1 hiPSC-derived neuroprogenitor cells were differentiated and harvested for protein exactly as previously described using three separate healthy control patient iPSCs [6]. Protein lysates were frozen prior to BCA protein quantification and preparation for the Simple Wes assay. Additionally, a subset of cells was fixed with ice-cold methanol for 15 minutes at −20 °C and immunocytochemistry was performed to ensure all cultures expressed Islet-1.

2.4 Immunoblot analysis

Protein samples were prepared by scraping cells into ice-cold PBS, centrifuging, and adding RIPA buffer containing protease (Sigma-Aldrich, St. Louis, MO) and phosphatase inhibitor cocktails 2 & 3 (Sigma, Sigma-Aldrich, St. Louis, MO) to the pellet. After gentle homogenization, cells were centrifuged at 4°C for 10 minutes at 20,000 *g*. The resulting DNA containing pellet was removed from the lysate, and the protein concentration was quantified using the BCA assay (Peirce Technologies) with a BSA standard curve. Samples were mixed with 5× SDS loading buffer containing 1% 2-mercaptoethanol and boiled for 5 minutes. 15 μg of protein was loaded for each sample onto a 4–15% pre-cast gel SDS-PAGE gel (BioRad, Hercules, CA) and run at 90V for 120 minutes. The protein bands were then transferred onto nitrocellulose membranes using iBlot Gel Transfer Device (Life Technologies). The remaining gel was stained with IRDye Blue protein stain (LI-COR, Lincoln, NE). Since the gels retained ~1/3 of the original protein after transferring with the iBlot, the stained gels were imaged on the Li-Cor Odyssey Imaging System and the intensity of the entire lane from ~150-20 kDa was quantified. This value was used to normalize the values of immunostained bands. The membrane was blocked in Odyssey Blocking Buffer for one hour prior to the addition of the primary antibodies. The primary antibodies were diluted 1:1000 in Odyssey Blocking Buffer containing 0.1% TWEEN and incubated overnight. After washing 5 times for 5 minutes in TBST, membranes were incubated with secondary antibodies at 1:10,000 (LiCor, Lincoln, NE) for 1 hour. Membranes were imaged using the Li-Cor Odyssey Imaging System, and quantification was performed using Image Studio Lite (LiCOR, Lincoln, NE).

2.5 In-Cell Western Assay

Cells were plated in 96-well μClear black-walled plates (Greiner Bio-One, Frickenhausen, Germany) at the appropriate density for the particular line. After exposing cells to toxicants, cells were washed once in room temperature PBS (without calcium and magnesium). The cells were then fixed with 4% paraformaldehyde in PBS for 30 minutes at room temperature, washed 5 times for in PBS with 0.1% Triton-X 100, and blocked for 1.5 hours in 150 μL of Odyssey blocking buffer. Cells were then incubated with primary antibody at 1:400 in Odyssey blocking buffer (LiCor, Lincoln, NE) with 50 μL per well for 2.5 hours. After washing 4 times in PBS with 0.1% Tween-20 for 5 minutes, cells were incubated for 1 hour in the appropriate LiCor IRdye 800 secondary antibody at 1:800 dilution in Odyssey blocking buffer along with 1:500 of CellTag normalization dye (LI-COR, Lincoln, NE). An additional round of 5 washes for 5 minutes in PBS with Tween-20 was performed after which all buffer was removed. Plates were imaged with the Li-Cor Odyssey Imaging System

and intensities were calculated for each well with Image Studio software. Cultures that were not incubated with primary antibodies served as background. Antibody signals were normalized using the CellTag signal (a measure of total cells).

2.6 Cellular Fura-2 Manganese Extraction Assay (CFMEA)

CFMEA was performed as described previously [6].

2.7 Cell Titer Blue Cytotoxicity Assay

Mouse striatal cells (*STHdh*$^{Q7/Q7}$) were grown on 96-well plates. The day after replating, the cells were exposed to toxicants in the cell-type appropriate medium. After 22 hours of exposure, 20 μL of Cell Titer Blue reagent (Promega, Madison, WI) was added to each well. Prior to this addition, cell lysis buffer was added to several wells to provide an accurate fluorescence background for 0% viable cells. The plates were then incubated for 2 hours at 33° C. Fluorescence was measured using excitation of 570 nm and emission of 600 nm on a microplate reader.

2.8 Protein Simple Wes Protein Expression Quantification

The Protein Simple Wes (Protein Simple, San Jose, California) was performed on day 11 Islet-1 striatal neuroprogenitors derived from hiSPCs. The assays were performed following manufacturer's guidelines using the 12–230 kD kit: separation time= 25 min, voltage= 375volts, antibody diluent time= 5min, primary incubation time= 30min, and secondary antibody time= 30min. 5ul of protein lysate at 1ug/uL was used per run, per sample. The p-p53 antibody was diluted 1:50 and actin was diluted 1:200 in 0.1× sample buffer provided by the manufacturer. Expression is given as relative chemiluminescence signal area under the curve at a particular peak.

2.9 Graphing and Statistical Analysis

To allow for appropriate post-hoc statistical analysis, western blots comparing SMIs vs Vehicle were normalized to vehicle. For this data, 95% confidence interval testing (GraphPad Prism 7) analysis was performed. Graphs comparing Mn-treated to SMI+Mn were normalized to vehicle. For this data, t-tests were performed using Microsoft Excel. All graphs were made using GraphPad Prism 7.

3 Results

3.1 KU55933 and KU60019 do not completely inhibit p-p53 in wild-type STHdh cells

Recently, our lab has shown that ATM kinase is responsible for the phosphorylation of p53 on serine 15 (p-p53) following exposure to sub-toxic (200μM) concentrations of Mn in human induced pluripotent stem cells (hiPSCs) differentiated into striatal-like neuroprogenitors. We found that 1μM KU55933 completely inhibits phosphorylation of p53 at serine 15 following a 200μM Mn exposure in hiPSC-derived Day 11 striatal neuroprogenitors. However, in E14-derived mouse striatal neuroprogenitors (STHdh), KU55933 does not completely inhibit p-p53 or p-H2AX expression (~50% decrease), two targets of ATM, following a 24 hour, 50μM Mn exposure even at 20μM, a concentration far

beyond the reported IC_{50} for ATM (Supplemental Figure 1A). Furthermore, KU60019, a more potent and specific derivative of KU559933, was unable to block Mn-induced p-p53 activity at 10μM as measured by In-cell western (Supplemental Figure 1B) [31]. Previous work in this cell model also revealed that 20μM KU55933 was unable to completely block H_20_2 (1 hour) induced p-p53 activity but could block the DNA mutagen neocarzinostatin (1 hour) induced p-p53 activity, suggesting that other kinases are responsible (at least, in part) for Mn induced p-p53 expression [6].

3.2 NU7441 and LY294002 inhibit p-p53 activation and Mn uptake at concentrations which inhibit PI3K

Given the contradictory results between the hiPSC and STHdh systems, we sought to explore whether alternative kinases act similarly to ATM in the STHdh cells to phosphorylate p53 at serine 15. Additionally, a previous study revealed that KU55933 can inhibit DNApk, mTOR, and PI3K at 2.5μM, 9.3μM and 16.6μM, respectively [32]. In order to determine if any of these kinase signaling pathways are responsible for Mn-induced phosphorylation of p53, we utilized several small molecule inhibitors (SMIs) with overlapping IC_{50s} for DNApk, mTOR, ATM, and PI3K (Table 1). As kinase inhibitors are notoriously nonspecific, we used other PIKK inhibitors that also inhibit PI3K at defined IC_{50s}, providing additional validation of our studies. In this way, we used overlapping, yet specific IC_{50s} to exclude particular protein targets (ie: If KU55933 were to inhibit Mn-induced p-p53 at 2.5 μM, but NU7441 does not inhibit p-p53 at 14nM and LY294002 does not inhibit at 1.2 μM, then DNApk inhibition would likely not be responsible for reduced p-p53– see Table 1). Thus, we first exposed STHdh cells for 24-hours with 50μM Mn and either NU7441 or LY294002. NU7441 is known to inhibit DNApk at 14nM, but also inhibits PI3K at 5 μM. LY294002 inhibits PI3K at 7 μM. Upon treatment with Mn and NU7441/LY294002, a ~50% decrease in p-p53 levels was observed with 5μM NU7441 and 7μM LY294002, mirroring the effects of 20μM KU55933 on p-p53 expression (Figure 1 A,B) [33, 34]. At these concentrations, NU7441 and LY294002 do not inhibit ATM. Furthermore, NU7441 and LY294002 reduced Mn-induced p-p53 levels in a dose-dependent manner with an approximate IC_{50} near their defined IC_{50} for PI3K (Figure 1 C, D).

3.3 LY294002, NU7441, KU55933, and KU60019 can reduce Mn uptake at concentrations near the IC_{50} for PI3K

It was surprising that PI3K inhibition reduced Mn-induced p-p53 expression, as PI3K is not directly linked to the activation of ATM/p53 (though downstream signaling members of PI3K—AKT and mTOR—have been linked to p53 regulation). We hypothesized that these inhibitors (LY294002, NU7441, KU55933, and KU60019) could be acting by reducing Mn uptake itself, thus reducing the intracellular pool of Mn and leading to a decrease in p-p53. Utilizing the cellular fura-2 Mn extraction assay (CFMEA), we examined Mn uptake after a 24-hour dual exposure/treatment with 50μM Mn and an SMI. LY294002, NU7441, KU55933, and KU60019 were able to reduce Mn uptake only at concentrations which neared the IC_{50} for PI3K inhibition (mTOR inhibitors had no effect on Mn uptake even at levels exceeding the IC_{50} for mTOR) (Figure 2). The two ATM inhibitors (KU55933 and KU60019) were able to inhibit Mn-induced p-p53 expression only at concentrations

exceeding the IC_{50} for ATM (Figure 2C, D). These data suggest that the observed reduction in Mn-induced p-p53 expression by these SMIs is a result of decreased Mn uptake.

3.4 LY294002 and NU7441 can reduce Mn-induced p-AKT and p-S6 expression at concentrations near the IC_{50} for PI3K

Mn exposure has been known to activate AKT and mTOR pathways in addition to ATM/p53 [2, 9–16, 35, 36]. STHdh cells were exposed with 50μM Mn and either NU7441, LY294002, or Rapamycin for 24-hours then expression levels of p-AKT(Ser473), and p-S6(Ser235/236) were analyzed by western blot. P-AKT(Ser473) expression levels were greatly reduced after exposure with NU7441 and LY294002 (~3 fold) while Rapamycin was unable to inhibit p-AKT levels (Figure 3A, C), consistent with mTORC1 signaling being downstream of AKT. p-S6 (Ser235/236) levels, indicative of mTOR activity, were reduced to the greatest magnitude after NU7441 or LY294002 exposure, but also after exposure with 1nM rapamycin (Figure 3B, D). We examined the effects of LY294002, NU7441, and Rapamycin without Mn (from the same set as data in Figure 3A–D) which show that mTOR is blocked by LY294002, high concentrations of NU7441 which should inhibit PI3K, and rapamycin. LY294002 and NU7441, but not rapamycin, reduced expression of p-AKT, consistent with their inhibitory cross-reactivity for PI3K. None of the inhibitors blocked basal p-p53 expression (Supplemental Figure 2). We observed similar phospho-protein trends after 3 hour exposures but neither LY294002 nor NU7441 could reduce Mn uptake after only 3 hours (Supplemental Figure 3). These results confirm that the SMIs are inhibiting the pathways we expected, further confirming a role for PI3K in Mn homeostasis and Mn-dependent cell signaling in this STHdh cell line.

3.5 LY294002 is unable to reduce Mn uptake in other cell lines or during shorter exposures

We next investigated whether the inhibition of PI3K also had an effect on Mn uptake in other cell models aside from STHdh. Additionally, given that PI3K is a critical protein involved in both endocytic and exocytic trafficking as well as activation of AKT, we wanted to examine whether the observed effects on Mn uptake are driven by cellular toxicity. We exposed STHdh cells with Mn and/or LY294002, NU7441, KU55933, or KU60019 for 24 hours and used Cell Titer Blue to measure cell viability. Cell viability in the STHdh was relatively unchanged by exposure/treatment with Mn and/or inhibitors (Figure 4B, C). However, while STHdh cells exhibit robust decreases in net Mn uptake following dual Mn and PI3K inhibitor exposure with limited toxicity, PI3K inhibition was unable to reduce Mn uptake in any of the other cell lines tested (ST14A, Mouse embryonic fibroblasts (MEF), hiPSC differentiated striatal neuroprogenitors) (Figures 4A, D). We also tested whether LY294002 and NU7441 could inhibit PI3K signaling (p-AKT, p-S6 expression) during 3 or 24 hour exposures in Neuro2A and HEK293 cells. We found that LY294002 blocks basal (~50%) and Mn-induced AKT/mTOR activity in these cell lines after 3 or 24 hours, but both LY294002 and NU7441 do not block Mn uptake (Figure 5, 6, Supplemental Figure 4). These data suggest the mechanism for PI3K inhibition on net Mn uptake is not sufficiently explained by AKT or S6 signaling and is specific to the unique biology of the STHdh cell line.

3.6 LY294002 inhibits p-p53 activity in STHdh cells by reducing intracellular Mn

As we observed decreased net Mn uptake with LY294002 and Mn co-exposure, we postulated that the PI3K inhibitor decreases Mn-induced increased p-p53 levels by decreasing intracellular Mn levels. Consequently, we assessed the relationship of intracellular Mn levels and p-p53 levels at a range of Mn exposures (25, 37.5, and 50μM) with and without LY294002 (7μm). LY294002 reduced intracellular Mn and p-p53 expression by 50% at all Mn concentrations. Furthermore, a linear regression of Mn vs. p-p53 activity reveals a high correlation between Mn levels and Mn-induced p-p53 expression (R^2=0.9649, 0.9860, and 0.9775 for Mn, Mn and LY294002, combined Mn and Mn LY294002 values, respectively) (Figure 7A–C). In addition, ANCOVA analysis was performed on this data to examine whether these linear regression lines were statistically different from each other. ANCOVA revealed that the slopes of the regression lines were not statistically different and were heavily correlated (R^2=0.98, p=0.218, df=6, F=1.98). These exposures resulted in slight reductions in cell viability, but not enough to account for the observed changes in Mn uptake and p-p53 expression (Figure 7D). Together these data suggest p-p53 acts as a surrogate rheostat of Mn levels within these cells. Together, these findings confirm our hypothesis that LY294002 reduces intracellular Mn, indirectly reducing activation of p-p53 by Mn, rather than inhibiting direct phosphorylation of p53 by PI3K or a downstream partner.

3.7 PI3K inhibition does not block Mn-induced p-p53 in Day 11 Islet 1 hiPSC-derived Neuroprogenitors

Lastly, we sought to test whether LY294002 inhibits Mn-induced increases in p-p53 in a cell line where LY294002 is unable to reduce Mn uptake (day 11 hiPSC-derived Islet-1 striatal neuroprogenitors). Dual LY294002 and 200μM Mn exposure did not block Mn-induced p-p53 activity (p=0.145) in three patient-derived cell lines (Figure 8B, C). As a positive control, KU60019 was able to partially reduce Mn-induced p-p53 levels at 1μM (p=0.047), but to a lesser degree than previous reports of KU55933 at 1μM in these same cells. The effect of KU55933 was confirmed in this study (Figure 8A). Together, these data suggest PI3K plays a unique role in Mn uptake, and thus Mn-induced cell signaling activity, in STHdh cells but not other cell lines— even those of striatal lineage.

4 Discussion

We have demonstrated that the SMIs KU-55933, NU-7441, and LY294002 can potently inhibit Mn uptake (near ~50% for all three SMIs) in a mouse striatal neuroprogenitor model at concentrations consistent with inhibition of their shared target, PI3K. KU-60019, to the best of our knowledge, has not been reported to inhibit PI3K, though KU55933 is known to inhibit PI3K at concentrations of 16.6uM or higher. Our data suggest that KU-60019 also inhibits PI3K at an approximate IC_{50} of 10μM (Figure 2D), if it reduces net intracellular Mn uptake in STHdh cells via the same mechanisms the other SMIs used. This conclusion is consistent with the relative inhibition of Mn-uptake for KU-60019 being almost identical (~50%) to the established PI3K inhibitors. Our data suggest KU-55933, NU-7441, LY294002, and KU-60019 do not decrease net Mn levels via reduced cell viability, since effective concentrations only showed about a 15–20% reduction in viability, even in the

presence of Mn - this was insufficient to account for the over 50% decrease in Mn uptake seen with these inhibitors. LY294002, a specific inhibitor of PI3K, is effective at reducing net Mn uptake at a concentration consistent with PI3K inhibition from the literature (7μM) (Figure 3) [37]. Likewise, the concentrations at which NU-7441 and KU-59933 were found to be effective at inhibiting Mn uptake and p-p53 expression (5μM and 20μM, respectively) are also consistent with inhibition of their shared off-target, PI3K (inhibited at 5μM and 16.6μM, respectively) (Table 1, Figure 3). mTORC1 is also a shared target between all four inhibitors, but use of mTORC1 inhibitors rapamycin or torin at concentrations equal to or surpassing their IC_{50s} for mTORC1 had no effect on Mn uptake (Figure 2E) [38, 39].

As LY294002 could not reduce Mn uptake in the other cell lines tested, the role of PI3K may be uniquely tied to Mn homeostasis in STHdh cells. Perhaps STHdh cells lack a compensatory pathway for PI3K that is preserved in the other cells tested, making STHdh Mn homeostasis exquisitely sensitive to PI3K inhibition. It is also possible the STHdh cell line, because its specific lineage, neuronal maturity, origin, etc. expresses a specific transporter which is PI3K dependent. Alternatively, while LY294002 is reported to be specific to PI3K at the concentrations used, it is possible that LY294002 is also inhibiting another protein, similar to PI3K, in STHdh cells and causal in the observed effects. Reported IC_{50s} of LY294002 for PI3K have been somewhat variable between studies and cell lines (1–10μM). These reports have shown that LY294002 can also inhibit other targets (including mTOR and DNApk) at concentrations lower than 10μM [34, 40, 41]. However, in this study we utilized more specific inhibitors (Rapamycin and NU7441) with overlapping IC_{50s}, suggesting that neither mTOR nor DNApk are responsible for the effect. Collectively, available data cannot exclude the possibility that a specific off-target for LY294002, aside from mTOR and DNApk, may be uniquely expressed in STHdh cells and responsible for Mn uptake in these cells and not in other cell lines. However, this specific off-target would have to be coincidentally inhibited by four different inhibitors at all their reported IC_{50s} for PI3K.

While our study does not elucidate the mechanism by which PI3K is modulating Mn uptake, our results do offer some insight. PI3K inhibition only results in reduced Mn uptake in STHdh cells after 24hrs, which could indicate an epigenetic alteration or a transcriptional-to-translational cascade is occurring in these cells after the addition of PI3K inhibitors, reducing Mn uptake (Figure 2, Supplemental Figure 3). However, these four inhibitors do inhibit basal and Mn-induced p-AKT and p-S6 expression at 3 hours, even in cell lines in which they do not affect Mn uptake (Figure 5, 6, Supplemental Figure 4). Thus, inhibition of AKT and mTOR is not responsible for the reduction in Mn uptake observed upon exposure with PI3K inhibitors. Furthermore, the results suggest that Mn-induced p-AKT and p-S6 signaling are PI3K-dependent.

Our observations reported here raise some very novel and interesting questions. How is PI3K exerting its role on Mn-homeostasis in the STHdh model? What types of transport/transporters is PI3K working through to impinge on Mn homeostasis? Given the inherent difficulty in studying Mn homeostasis due to poorly understood transport and sequestration, understanding how PI3K is capable of such a dramatic effect on Mn uptake could lead to the discovery of other, more commonly shared, pathways of Mn homeostasis. Considering PI3K's downstream role in endocytosis via signaling of PIP2-PIP3, a reasonable hypothesis

is that PI3K signaling upregulates endocytosis of a specific, unknown Mn-receptor on the cell surface. This type of transport would mirror clathrin-mediated endocytosis of iron, another biologically indispensable heavy metal. A previous study by our lab has shown that saturating clathrin-mediated uptake with iron, thus blocking transferrin-mediated Mn uptake, only reduces Mn toxicity by ~10% STHdh cells [7]. This suggests clathrin-mediated endocytosis cannot fully explain the effect of PI3K inhibition on Mn uptake. Regardless, Mn uptake has directly been associated with intracellular toxicity via increased generation of reactive oxygen species and mitochondrial dysfunction and has been recognized as a potent neurotoxicant—particularly in dopaminergic neurons [42–51]. This study suggests that PI3K may play a role in neuronal Mn homeostasis, offering a potential target/pathway which can be furthered studied in the context of Mn toxicity. LY294002 causes some toxicity, which is exacerbated by addition of toxic concentrations of Mn and, thus, does not reduce overall intracellular toxicity. In principle, however, using other small molecules to target pathways/proteins (possibly including PI3K) that can reduce Mn uptake in the context of toxic Mn exposures could be valuable tools for studying future therapeutics.

Similarly, given PI3K is upstream of AKT/mTOR, it is possible that PI3K is responsible for perpetuating an upstream signal leading to the activation of autophagy via the mTOR pathway, which may then act to degrade Mn-laden proteins, releasing Mn into a useable pool for the cell. However, the lack of effect on Mn uptake by rapamycin and Torin, known mTOR inhibitors, do not support this hypothesis. If PI3K does truly exert such potent control on Mn homeostasis, it could also control activation of the wide array of Mn-dependent and Mn-activated enzymes and thus, Mn-dependent cell signaling. In this study, we have shown that p-p53 expression is tightly correlated to Mn status in this cell line and that PI3K can act to modulate this ion-protein interaction (Figure 7). Furthermore, PI3K's protein-serine kinase activity is Mn-dependent while its lipid activity is inhibited by Mn [52]. Indeed, responding as a Mn "sensor", PI3K could function to regulate not only the ATM/p53 and AKT/mTOR pathways, but many other Mn-responsive processes within the cell, in response to intracellular Mn levels.

Supplementary Material

Refer to Web version on PubMed Central for supplementary material.

Acknowledgments

We would like to thank Dr. Kevin Ess and his lab for providing Rapamycin and Torin2 inhibitors and for thoughtful discussion. We thank Dr. Anthony Tharp of the VBI core facilities for equipment and technical support. We thank Dr. Bingying Han for her dedicated iPSC maintenance. HEK293 cells were generously donated by Audra Foshage of the Tansey lab. This work was supported by the National Institutes of Health [NIH/NIEHS RO1 ES016931 (ABB) and RO1 ES010563 (ABB and MA)].

References

1. Aschner M, et al. Manganese and its Role in Parkinson's Disease: From Transport to Neuropathology. NeuroMolecular Medicine. 2009; 11(4):252–266. [PubMed: 19657747]
2. Dieter HH, Bayer TA, Multhaup G. Environmental Copper and Manganese in the Pathophysiology of Neurologic Diseases (Alzheimer's Disease and Manganism). Acta hydrochimica et hydrobiologica. 2005; 33(1):72–78.

3. Kwakye GF, et al. Manganese-Induced Parkinsonism and Parkinson's Disease: Shared and Distinguishable Features. International journal of environmental research and public health. 2015; 12(7):7519–7540. [PubMed: 26154659]
4. Horning KJ, et al. Manganese Is Essential for Neuronal Health. Annual review of nutrition. 2015; 35:71–108.
5. Kwakye GF, Li D, Bowman AB. Novel high-throughput assay to assess cellular manganese levels in a striatal cell line model of Huntington's disease confirms a deficit in manganese accumulation. NeuroToxicology. 2011; 32(5):630–639. [PubMed: 21238486]
6. Tidball AM, et al. A novel manganese-dependent ATM-p53 signaling pathway is selectively impaired in patient-based neuroprogenitor and murine striatal models of Huntington's disease. Human Molecular Genetics. 2015; 24(7):1929–1944. [PubMed: 25489053]
7. Williams BB, et al. Altered Manganese Homeostasis and Manganese Toxicity in a Huntington's Disease Striatal Cell Model Are Not Explained by Defects in the Iron Transport System. Toxicological Sciences. 2010; 117(1):169–179. [PubMed: 20547568]
8. Tidball AM, Bichell T, Bowman AB. Manganese in Health and Disease. rsc. 2015:540–573.
9. Bae J-H, et al. Manganese induces inducible nitric oxide synthase (iNOS) expression via activation of both MAP kinase and PI3K/Akt pathways in BV2 microglial cells. Neuroscience letters. 2006; 398(1–2):151–154. [PubMed: 16417967]
10. Cordova FM, et al. Manganese-exposed developing rats display motor deficits and striatal oxidative stress that are reversed by Trolox. Archives of toxicology. 2013; 87(7):1231–1244. [PubMed: 23385959]
11. Cordova FM, et al. In vivo manganese exposure modulates Erk, Akt and Darpp-32 in the striatum of developing rats, and impairs their motor function. PloS one. 2012; 7(3)
12. Dearth RK, et al. Prepubertal exposure to elevated manganese results in estradiol regulated mammary gland ductal differentiation and hyperplasia in female rats. Experimental Biology and Medicine. 2014; 239(7):871–882. [PubMed: 24845367]
13. Dormond O, et al. Manganese-induced integrin affinity maturation promotes recruitment of alpha V beta 3 integrin to focal adhesions in endothelial cells: evidence for a role of phosphatidylinositol 3-kinase and Src. Thrombosis and haemostasis. 2004; 92(1):151–161. [PubMed: 15213856]
14. Exil V, et al. Activation of MAPK and FoxO by manganese (Mn) in rat neonatal primary astrocyte cultures. PloS one. 2014; 9(5)
15. Srivastava VK, Hiney JK, Dees WL. Manganese stimulated Kisspeptin is mediated by the Insulin-like growth factor-1/Akt/ mammalian target of rapamycin pathway in the prepubertal female rat. Endocrinology. 2016
16. Williams BB, et al. Disease-toxicant screen reveals a neuroprotective interaction between Huntington's disease and manganese exposure. Journal of neurochemistry. 2010; 112(1):227–237. [PubMed: 19845833]
17. Ma X, et al. Involvement of dysregulated Wip1 in manganese-induced p53 signaling and neuronal apoptosis. Toxicology Letters. 2015; 235(1):17–27. [PubMed: 25791630]
18. Wan C, et al. Pivotal roles of p53 transcription-dependent and -independent pathways in manganese-induced mitochondrial dysfunction and neuronal apoptosis. Toxicology and Applied Pharmacology. 2014; 281(3):294–302. [PubMed: 25448048]
19. Guilarte TR. APLP1, Alzheimer's-like pathology and neurodegeneration in the frontal cortex of manganese-exposed non-human primates. NeuroToxicology. 2010; 31(5):572–574. [PubMed: 20188756]
20. Guilarte TR, et al. Increased APLP1 expression and neurodegeneration in the frontal cortex of manganese-exposed non-human primates. Journal of Neurochemistry. 2008; 105(5):1948–1959. [PubMed: 18284614]
21. Humbert S, et al. The IGF-1/Akt Pathway Is Neuroprotective in Huntington's Disease and Involves Huntingtin Phosphorylation by Akt. Developmental Cell. 2002; 2(6):831–837. [PubMed: 12062094]
22. Humbert S, Saudou F. Huntingtin phosphorylation and signaling pathways that regulate toxicity in Huntington's disease. Clinical Neuroscience Research. 2003; 3(3):149–155.

23. Lopes C, et al. IGF-1 intranasal administration rescues Huntington's disease phenotypes in YAC128 mice. Molecular neurobiology. 2014; 49(3):1126–1142. [PubMed: 24347322]
24. Naia L, et al. Activation of IGF-1 and insulin signaling pathways ameliorate mitochondrial function and energy metabolism in Huntington's Disease human lymphoblasts. Molecular neurobiology. 2015; 51(1):331–348. [PubMed: 24841383]
25. Ribeiro M, et al. Insulin and IGF-1 improve mitochondrial function in a PI-3K/Akt-dependent manner and reduce mitochondrial generation of reactive oxygen species in Huntington's disease knock-in striatal cells. Free radical biology & medicine. 2014; 74:129–144. [PubMed: 24992836]
26. Yamamoto A, Cremona ML, Rothman JE. Autophagy-mediated clearance of huntingtin aggregates triggered by the insulin-signaling pathway. The Journal of cell biology. 2006; 172(5):719–731. [PubMed: 16505167]
27. Lee JH, et al. Reinstating aberrant mTORC1 activity in Huntington's disease mice improves disease phenotypes. Neuron. 2014; 85(2):303–315. [PubMed: 25556834]
28. Sarkar S, et al. Rapamycin and mTOR-independent autophagy inducers ameliorate toxicity of polyglutamine-expanded huntingtin and related proteinopathies. Cell death and differentiation. 2008; 16(1):46–56. [PubMed: 18636076]
29. Williams A, et al. Novel targets for Huntington's disease in an mTOR-independent autophagy pathway. Nature Chemical Biology. 2008; 4(5):295–305. [PubMed: 18391949]
30. Chan DW, et al. Purification and characterization of ATM from human placenta. A manganese-dependent, wortmannin-sensitive serine/threonine protein kinase. The Journal of biological chemistry. 2000; 275(11):7803–7810. [PubMed: 10713094]
31. Golding SE, et al. Improved ATM kinase inhibitor KU-60019 radiosensitizes glioma cells, compromises insulin, AKT and ERK prosurvival signaling, and inhibits migration and invasion. Molecular Cancer Therapeutics. 2009; 8(10):2894–2902. [PubMed: 19808981]
32. Hickson I, et al. Identification and characterization of a novel and specific inhibitor of the ataxia-telangiectasia mutated kinase ATM. Cancer research. 2004; 64(24):9152–9159. [PubMed: 15604286]
33. Leahy J, et al. Identification of a highly potent and selective DNA-dependent protein kinase (DNA-PK) inhibitor (NU7441) by screening of chromenone libraries. Bioorganic & Medicinal Chemistry Letters. 2004; 14(24):6083–6087. [PubMed: 15546735]
34. Vlahos CJ, et al. A specific inhibitor of phosphatidylinositol 3-kinase, 2-(4-morpholinyl)-8-phenyl-4H-1-benzopyran-4-one (LY294002). The Journal of biological chemistry. 1994; 269(7): 5241–5248. [PubMed: 8106507]
35. Hiney JK, Srivastava VK, Dees WL. Manganese induces IGF-1 and cyclooxygenase-2 gene expressions in the basal hypothalamus during prepubertal female development. Toxicological sciences : an official journal of the Society of Toxicology. 2011; 121(2):389–396. [PubMed: 21402727]
36. Srivastava VK, Hiney JK, Dees WL. Early Life Manganese Exposure Upregulates Tumor-Associated Genes in the Hypothalamus of Female Rats: Relationship to Manganese-Induced Precocious Puberty. Toxicological Sciences. 2013; 136(2):373–381. [PubMed: 23997110]
37. Bar J, et al. The PI3K inhibitor LY294002 prevents p53 induction by DNA damage and attenuates chemotherapy-induced apoptosis. Cell Death & Differentiation. 2005; 12(12):1578–1587. [PubMed: 15933740]
38. Liu Q, et al. Characterization of Torin2, an ATP-Competitive Inhibitor of mTOR, ATM, and ATR. Cancer Research. 2013; 73(8):2574–2586. [PubMed: 23436801]
39. Thoreen CC, et al. An ATP-competitive Mammalian Target of Rapamycin Inhibitor Reveals Rapamycin-resistant Functions of mTORC1. Journal of Biological Chemistry. 2009; 284(12): 8023–8032. [PubMed: 19150980]
40. Brunn GJ, et al. Direct inhibition of the signaling functions of the mammalian target of rapamycin by the phosphoinositide 3-kinase inhibitors, wortmannin and LY294002. The EMBO journal. 1996; 15(19):5256–5267. [PubMed: 8895571]
41. Ballou LM, et al. Inhibition of mammalian target of rapamycin signaling by 2-(morpholin-1-yl)pyrimido[2,1-alpha]isoquinolin-4-one. The Journal of biological chemistry. 2007; 282(33): 24463–24470. [PubMed: 17562705]

42. Brouillet EP, et al. Manganese Injection into the Rat Striatum Produces Excitotoxic Lesions by Impairing Energy Metabolism. Experimental Neurology. 1993; 120(1):89–94. [PubMed: 8477830]
43. Guilarte TR. Manganese and Parkinson's Disease: A Critical Review and New Findings. Environmental Health Perspectives. 2010; 118(8):1071–1080. [PubMed: 20403794]
44. Neal AP, Guilarte TR. Mechanisms of lead and manganese neurotoxicity. Toxicology Research. 2013; 2(2):99–114. [PubMed: 25722848]
45. Zhang D, et al. Effects of manganese on tyrosine hydroxylase (TH) activity and TH-phosphorylation in a dopaminergic neural cell line. Toxicology and Applied Pharmacology. 2011; 254(2):65–71. [PubMed: 21310168]
46. An MC, et al. Genetic correction of Huntington's disease phenotypes in induced pluripotent stem cells. Cell stem cell. 2012; 11(2):253–263. [PubMed: 22748967]
47. Zhang S, Fu J, Zhou Z. In vitro effect of manganese chloride exposure on reactive oxygen species generation and respiratory chain complexes activities of mitochondria isolated from rat brain. Toxicology in Vitro. 2004; 18(1):71–77. [PubMed: 14630064]
48. Zhang S, Zhou Z, Fu J. Effect of manganese chloride exposure on liver and brain mitochondria function in rats. Environmental Research. 2003; 93(2):149–157. [PubMed: 12963399]
49. Gavin CE, Gunter KK, Gunter TE. Manganese and calcium transport in mitochondria: implications for manganese toxicity. Neurotoxicology. 1999; 20(2–3):445–453. [PubMed: 10385903]
50. Gunter TE, Gavin CE, Gunter KK. The case for manganese interaction with mitochondria. NeuroToxicology. 2009; 30(4):727–729.
51. Malecki EA. Manganese toxicity is associated with mitochondrial dysfunction and DNA fragmentation in rat primary striatal neurons. Brain Research Bulletin. 2001; 55(2):225–228. [PubMed: 11470319]
52. Chauhan V, et al. Phosphatidylinositol 3-kinase: Inhibition of intrinsic protein-serine kinase activity by phosphoinositides, and of lipid kinase activity by Mn2+ Biochimica et Biophysica Acta (BBA) - Molecular Cell Research. 1995; 1267(2–3):139–144. [PubMed: 7612667]

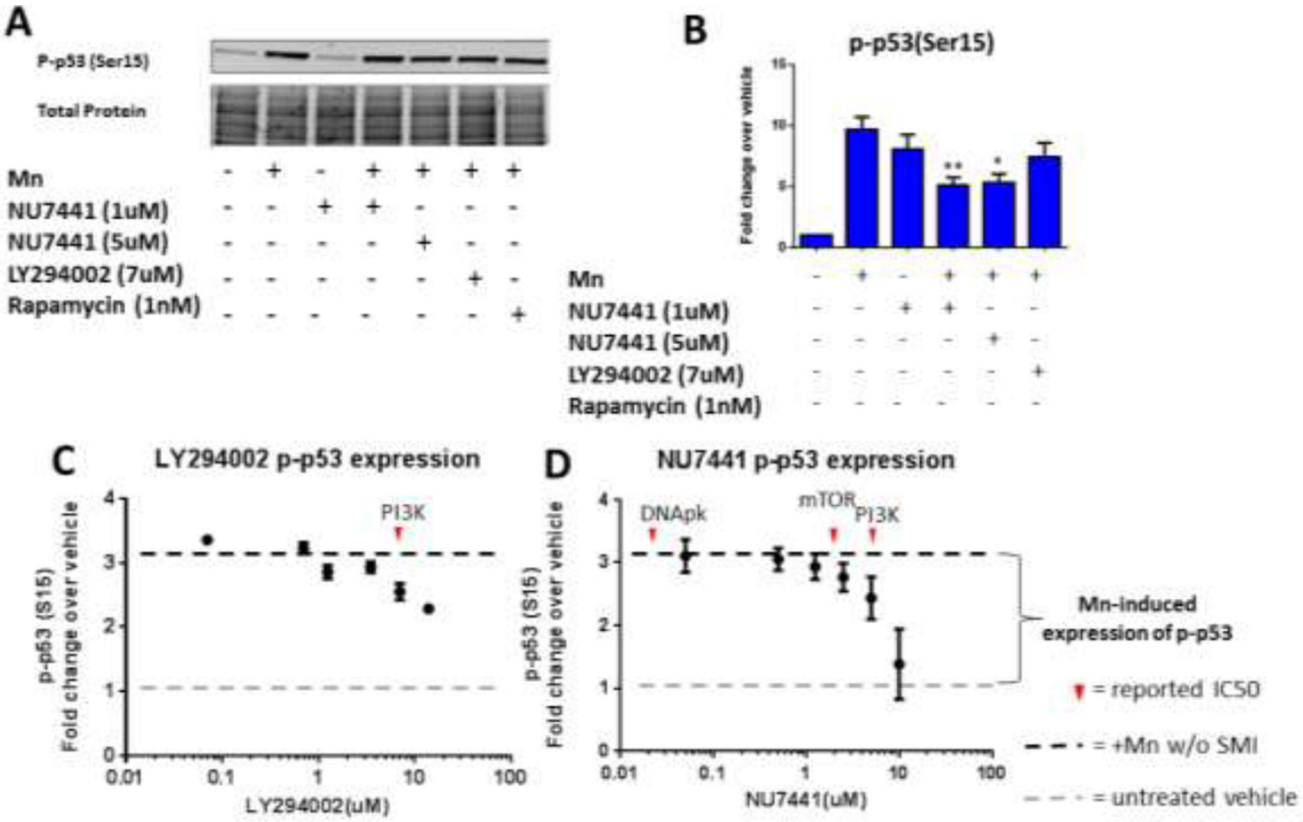

Figure 1. NU7441 and LY294002 inhibit phosphorylation of p53 activation and Mn uptake at concentrations that inhibit PI3K

A) Representative western blot showing p-p53 (ser15) expression in STHdh cells with added Mn and/or SMIs. Coomassie stain (total protein, below) was used as a loading control. **B)** Quantification of p-p53 (ser15) from western blots (n=3). Error bars=SEM.). All Mn + SMI values were compared with Mn alone by t-test. *p<0.05, **p<0.01. **C**, **D)** Dose-response curve for Mn-induced p-p53 expression using LiCor In-Cell Western assay with increasing concentrations of LY294002 or NU7441 (n=2 with 5 technical replicate wells, error bars represent SD of all 10 wells). Red arrows denote reported IC_{50} for respective SMI.

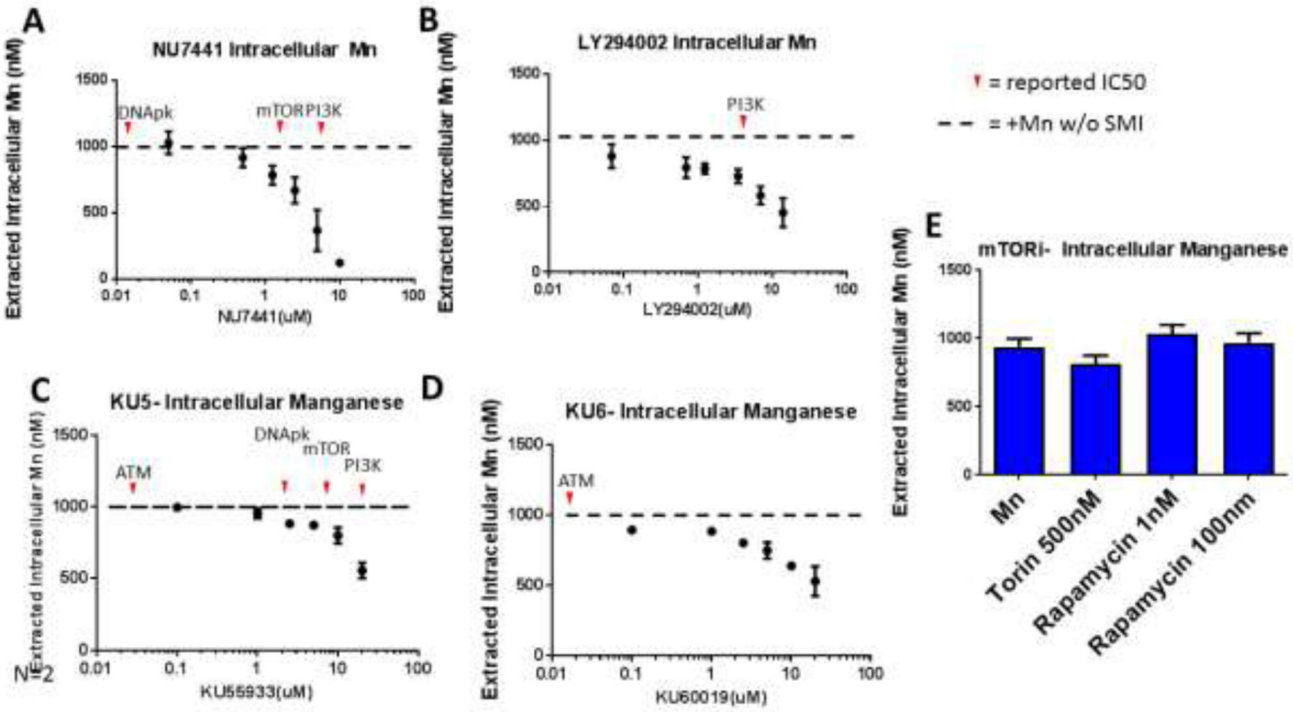

Figure 2. LY294002, NU7441, KU55933, and KU60019 can reduce Mn uptake at concentrations near the IC50 for PI3K

A–D) Cellular Fura-2 manganese extraction assay (CFMEA) was used to quantify 24-hour Mn uptake with increasing concentrations of NU7441, LY294002, KU55933, or KU60019. (n=3 with 6 technical replicate wells, error bars represent SD of 3 biological replicates). Red arrows denote reported IC_{50} for respective SMI. **E)** CFMEA after 24-hour Mn and/or mTOR inhibitors "mTORi" (Torin or Rapamycin).

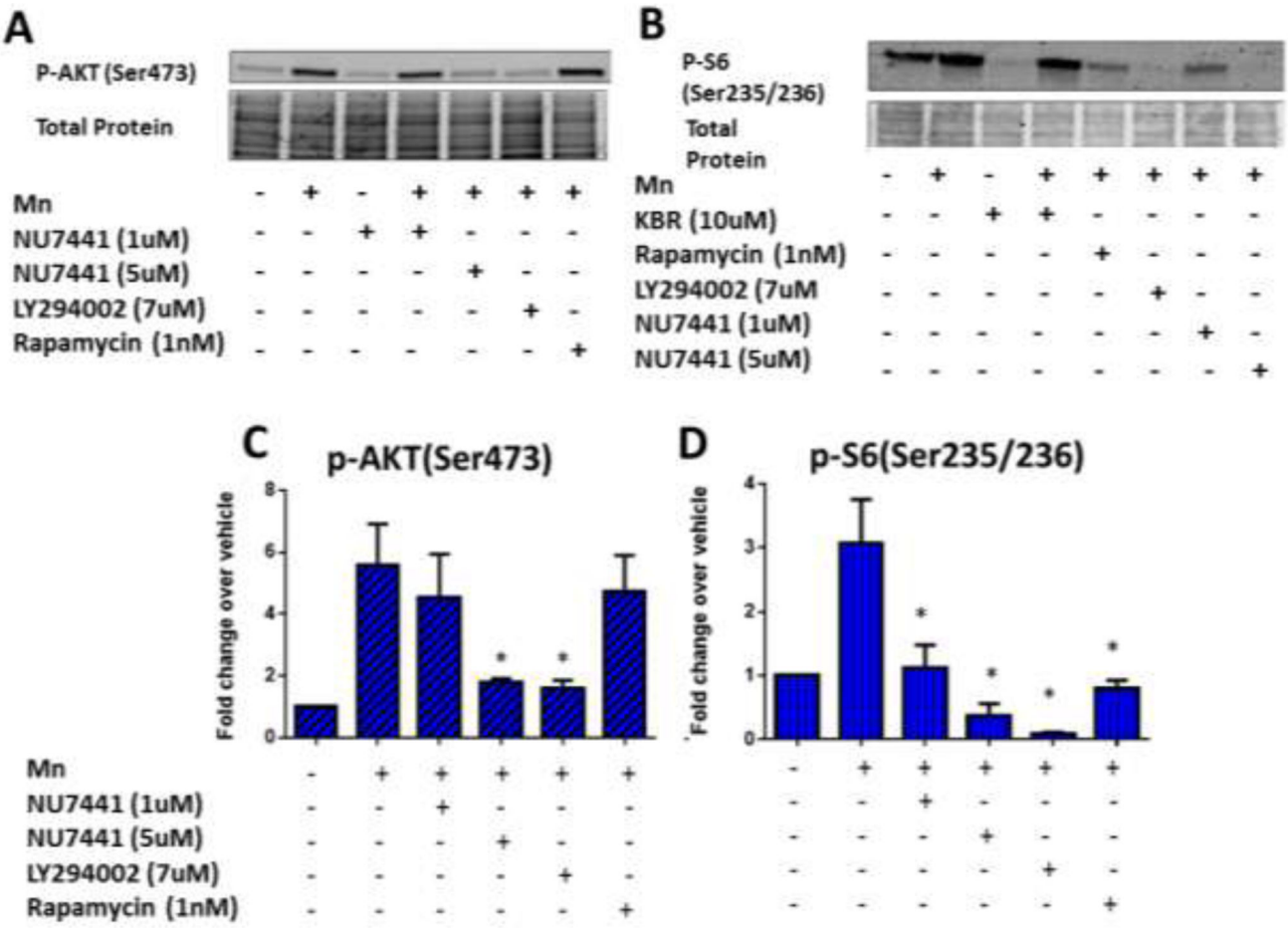

Figure 3. LY294002 and NU7441 can reduce Mn-induced p-AKT and p-S6 expression at concentrations near the IC50 for PI3K

A, B) Representative western blots for p-AKT(Ser473) or p-S6(Ser235/236) with Mn and/or SMI for 24 hours. Coomassie stain (total protein, below) was used as a loading control. **C,D)** Quantification of p-AKT(Ser473) or p-S6(Ser235/236) from western blots (n=3). All Mn + SMI values were compared with Mn alone by t-test. *p<0.05, **p<0.01. Error bars = SEM.

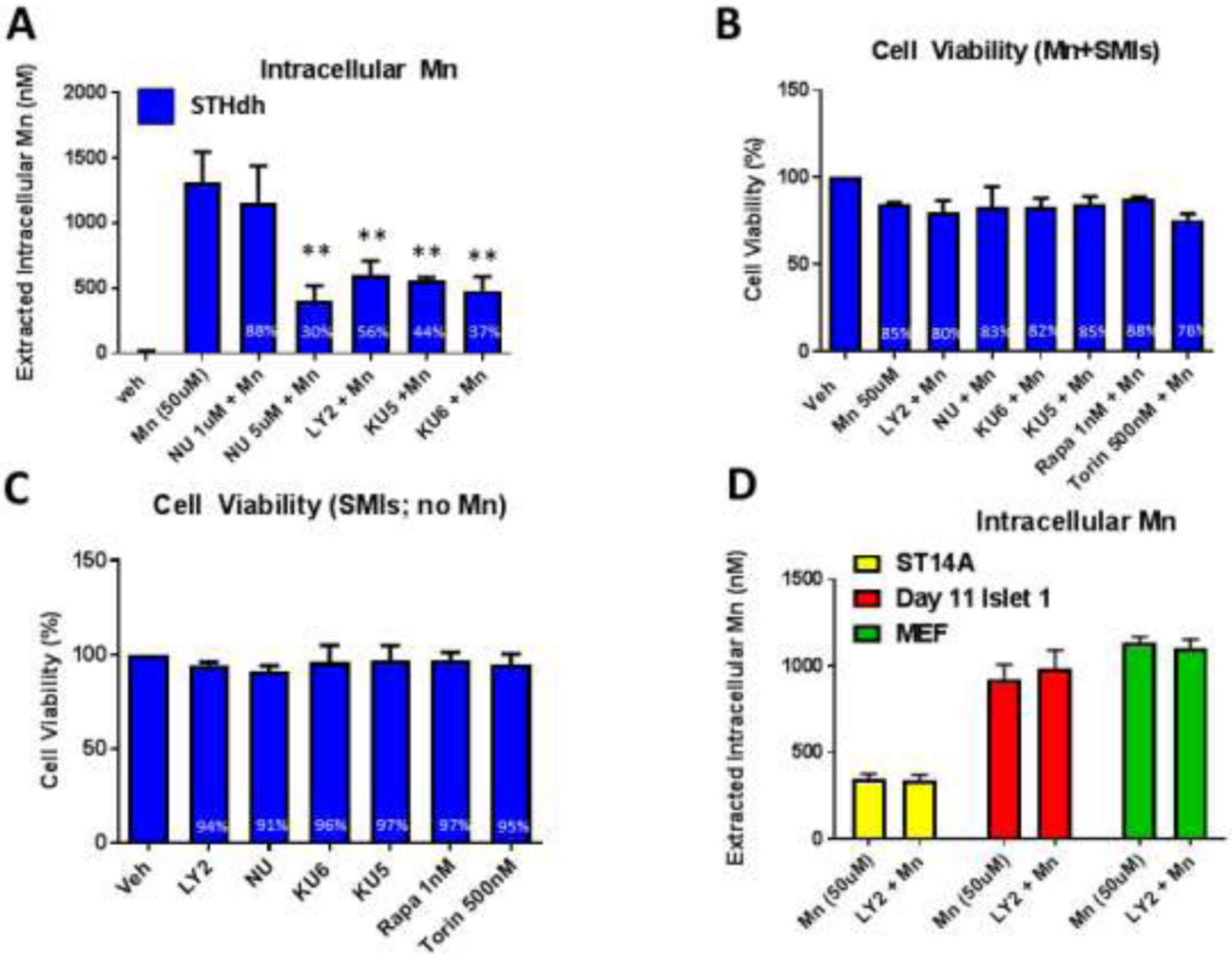

Figure 4. LY294002 is unable to reduce Mn uptake in other cell lines

A) CFMEA in STHdh cells after 24 hour exposure with Mn and/or SMIs. **B)** Cell Titer Blue viability assay after 24 hour exposure with Mn and SMIs. **C)** Cell Titer Blue viability assay after 24 hour exposure with SMIs only. **D)** CFMEA on other cell lines after 24 hour exposure with Mn or Mn+LY2. n=3 with 6 technical replicate wells each. All Mn + SMI values were compared with Mn alone by t-test. *p<0.05, **p<0.01. Error bars= SEM.

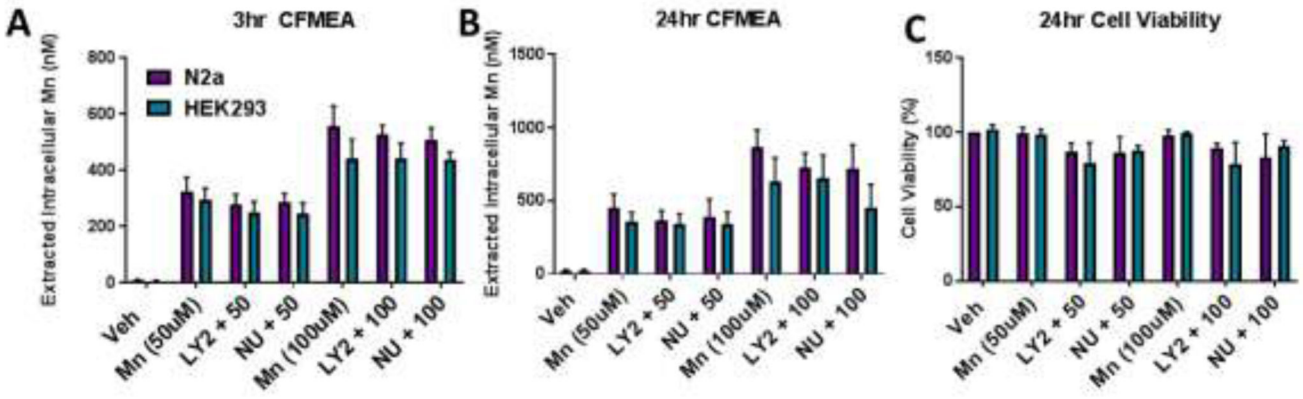

Figure 5. LY294002 and NU7441 do not decrease Mn uptake in Neuro2A (N2a) and HEK293 cells

CFMEA analysis after 3hr (**A**) or 24hr (**B**) dual exposure with 50μM or 100 μM Mn and 7μM or 5μM LY294002 or NU7441, respectively. **C)** Cell Titer Blue cell viability analysis after 24 hour exposures. n=3. All Mn + SMI values were compared with 50μM or 100μM Mn alone by t-test. *p<0.05, **p<0.01. Error bars= SEM.

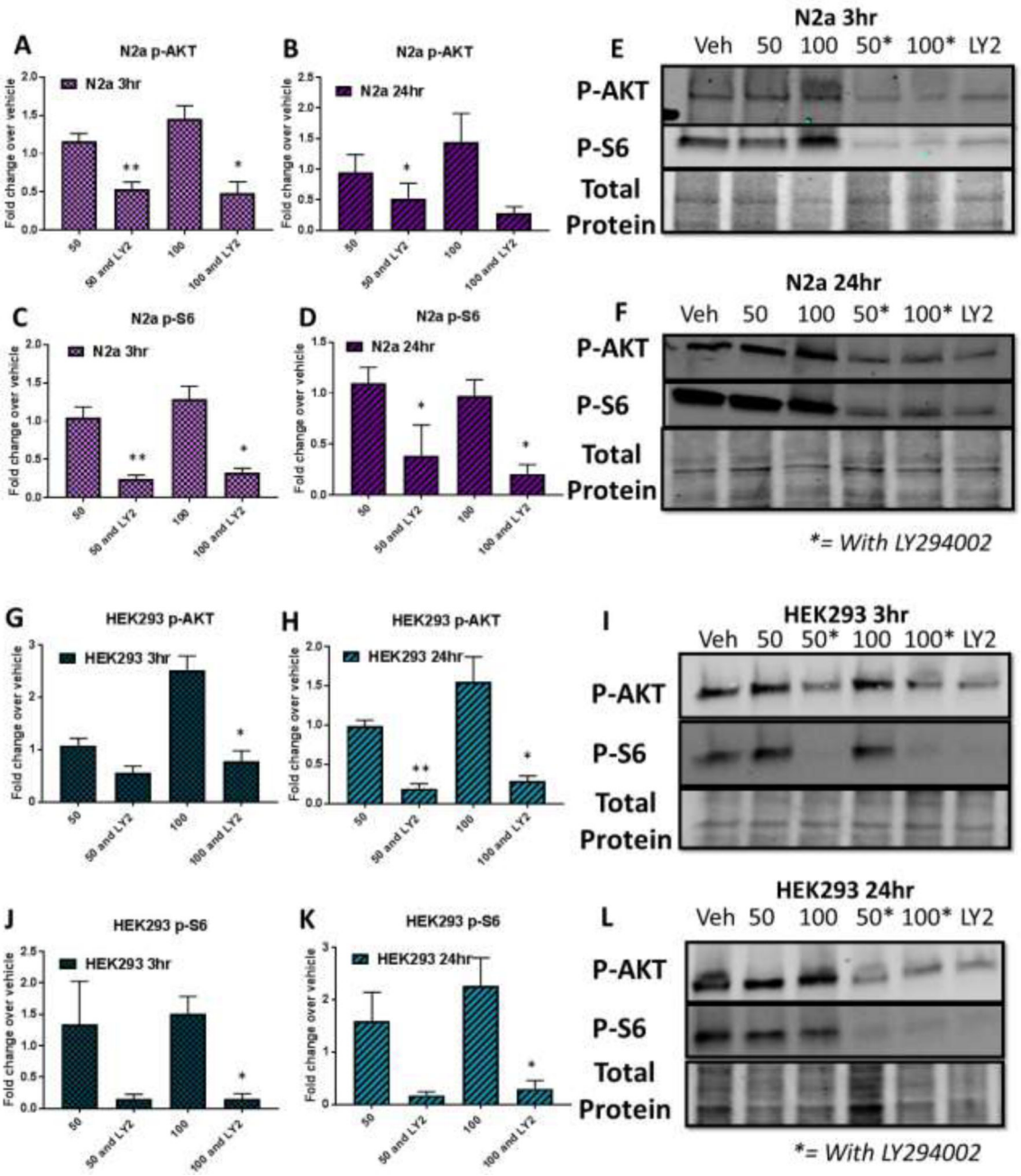

Figure 6. LY294002 inhibits Mn-induced p-AKT (Ser473) and p-S6 (Ser235/236) expression in Neuro2A (N2a) and HEK293 cells

Western blot analysis in Neuro2A (**A–F**) and HEK293 (**G–L**) cells after 3 or 24 hour dual exposures (50μM or 100μM Mn and 7μM LY294002). n=3. All Mn + SMI values were compared with 50μM or 100μM Mn alone by t-test. *p<0.05, **p<0.01. Error bars= SEM.

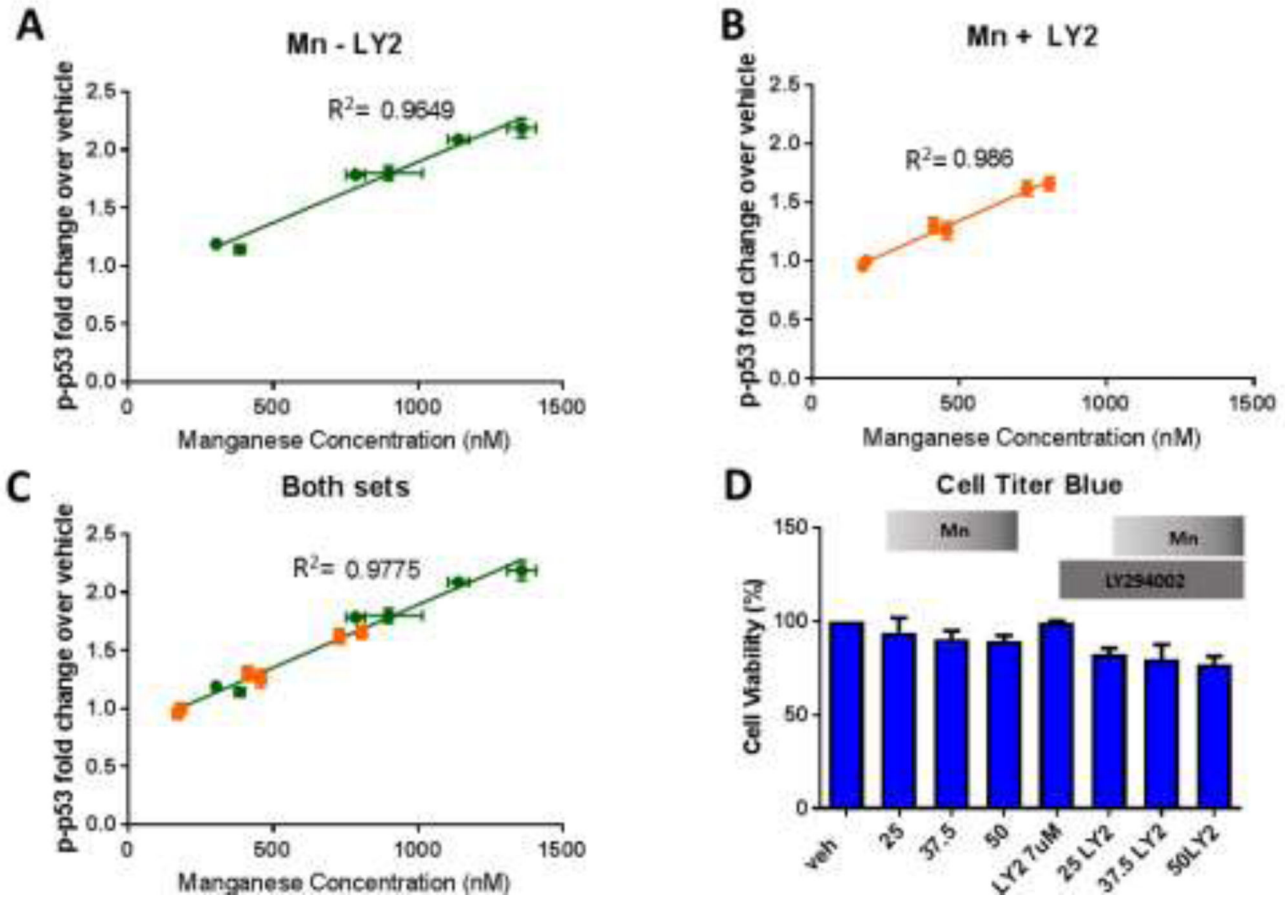

Figure 7. LY294002 inhibits p-p53 activity in STHdh cells by reducing intracellular Mn

A–C) Linear regression plots for Mn (X) vs p-p53 (Y) across 25μM, 37.5μM, or 50μM Mn exposures with or without LY2 for 24 hours. Mn **(A),** Mn+LY294002 **(B),** and Mn combined with Mn+LY2 **(C)** are plotted separately (n=2 with 5 replicate wells per condition, error bars are SD for each set of 5 replicate wells). R^2 values are shown next to each line. ANCOVA: R^2=0.98, p=0.218, df=2, F=1.98. **D)** Cell Titer Blue cell viability assay after 25μM, 37.5μM, or 50μM Mn exposure for 24 hours, with and without LY294002. Error bars= SEM.

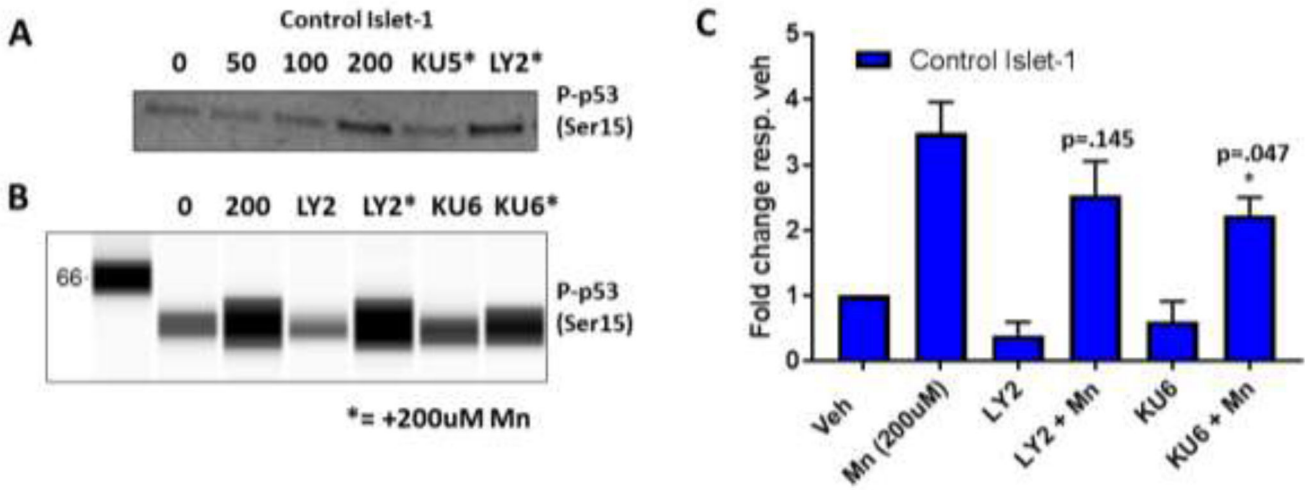

Figure 8. PI3K inhibition does not block Mn-induced p-p53 expression in Day 11 Islet 1 hiPSC-derived Neuroprogenitors

A) Representative western blot of confirmed complete inhibition of Mn-induced p-p53 activity after 24 hour treatment with Mn and 1μM KU50019. **B)** Representative Simple Wes "lane view" image of Islet-1 neuroprogenitor lysates – cells were treated with 200uM Mn and 7μM LY294002, or 1μM KU60019 with and without 200μM Mn – probed for p-p53 (Ser15). **C)** Quantification of Simple Wes for p-p53/actin and normalized to respective untreated vehicle. n=3 from three separate control hiPSC cell lines. All Mn + SMI values were compared with 50μM or 100μM Mn alone by t-test. *p<0.05, **p<0.01. Error bars= SEM.

Table 1

The literature reveals KU55933 inhibits PI3K at higher concentrations.

Inhibitor	PI3K	mTOR	ATM	ATR	DNApk
KU-55933	16.6μM[32]	9.3μM[32]	13nM[32]	100μM[32]	2.5μM[32]
KU-60019	Unknown[31]	Unknown[31]	6nM[31]	Unknown[31]	Unknown[31]
NU7441	5μM[33]	1.7μM[33]	100μM[33]	100μM[33]	14nM[33]
Rapamycin	--	.1nM[38,39]	--	--	--
Torin 2	1μM[38,39]	2nM[38,39]	.6μM[38,39]	35nM[38,39]	>1μM[38,39]
LY294002	1–10μM[34]	2.5μM[41]	>20μM[37]	>20μM[37]	1.2μM[40]

All inhibitors used in this study are shown below with known, reported IC_{50}s against PI3K, mTOR, ATM, ATR, and DNApk. Note citations in subscript.